Available online at www.sciencedirect.com
SCIENCE DIRECT®
Journal of Sound and Vibration 285 (2005) 1123–1149
JOURNAL OF SOUND AND VIBRATION
www.elsevier.com/locate/jsvi

Robust vibration isolation via frequency-shaped sliding control and modal decomposition

Lei Zuo, Jean-Jacques E. Slotine*

Department of Mechanical Engineering, Massachusetts Institute of Technology, 77 Massachusetts Ave., Cambridge, MA 02139-4307, USA

Received 10 April 2003; received in revised form 13 September 2004; accepted 16 September 2004
Available online 25 December 2004

Abstract

A robust controller design is proposed for multi-degree-of-freedom active vibration isolation, which accounts for plant uncertainties and payload disturbances using frequency-shaped sliding control. First, modal decomposition is employed to rewrite the MIMO vibration control problem as a combination of individual SISO control problems in modal coordinates. The modal parameters for decomposition and modelling can be extracted from theoretical or experimental modal analysis. Next, the target frequency-domain performance of isolation, in this case a skyhook model, is recast as a frequency-shaped sliding surface. The practical effects of boundary layer approximation in the resulting controller design are examined. Simulations illustrate that the ideal skyhook effect can indeed be robustly achieved. The frequency-shaped manifold is also extended to adaptive vibration isolation without using model reference. This algorithm has been recently verified by experiments (IEEE Transactions on Control Systems Technology (2005), in press), and has been demonstrated very effective for vibration isolation. The paper also shows, more generally, that the design of a frequency-shaped sliding surface is formally equivalent to a feedback–feedforward compensation problem. Nonlinear target dynamics of the same order as the nominal plant can also be attained.

*Corresponding author. Tel.: +1 617 253 0490; fax: +1 617 258 5802.
E-mail addresses: leizuo@mit.edu (L. Zuo), jjs@mit.edu (J.-J.E. Slotine).

0022-460X/$ - see front matter © 2004 Elsevier Ltd. All rights reserved.
doi:10.1016/j.jsv.2004.09.014

1. Introduction

Vibration isolation has been of great interest in the academic and industrial areas of precision machine tools, optical instruments, automobiles, aerospace, and civil structures. Passive isolators are often sufficient for high-frequency isolation in many applications. But damping tradeoffs exist between the isolation performance at high frequency and that at low frequency. Soft mounting is preferred for seismic vibration, but it causes static misalignment and dynamic instability under payload disturbances. To improve the performance (especially at low frequencies), active isolators are typically used.

Many configurations and control methods have been developed for the active isolation, such as linear control with velocity feedback [1,2], acceleration feedback [3], or force feedback [4], LQG/H2 control [5], and feedforward control [6].

In practice, since actual systems have many sources of uncertainties, robust controllers are required. H_∞ and μ-synthesis are used experimentally for robust active isolation [7]. Conventional sliding mode control has been used in base isolation of building structures [8,9]. Alleyne and Hedrick [10] and Kim and Ro [11] use the skyhook model as reference, and employ model-reference adaptive control and sliding control to track a given skyhook force or states. An adaptive sliding control algorithm has also been developed by Wang and Sinha [12] for multi-degree-of-freedom microgravity isolation, where the reference model is defined as an ideal transfer matrix.

To further enhance the isolation performance, multi-stage isolation may become necessary, combining passive and active stages [13,14]. Further uncertainties exist in such systems, which arise more challenges in system modelling and robust control. For instance, the mass, location, and dynamics of upper stages or the payload might be unknown or time-varying.

In this paper, we provide a practical approach for the control of MIMO isolation system with plant uncertainties and disturbances from upper stages through measurement-based (or analytical) modal decomposition and a novel sliding control strategy. In place of the standard sliding surfaces used in Refs. [8–12], we exploit *frequency-shaped* sliding surfaces, originally proposed in Ref. [15] for chattering attenuation, for shaping system performance directly in the frequency domain. Such a specification is quite natural for a skyhook dynamics target. The controller can be synthesized based on the data of experimental modal analysis, as well as a mathematical model.

The paper is organized as follows. Section 2 introduces modal analysis and decomposition. MIMO control of the isolation system can be handled with SISO systems in modal coordinates, with the residual coupling from other modes and payload dynamics taken as disturbances. In Section 3, frequency-shaped sliding control is used to achieve skyhook isolation under modal uncertainties and payload disturbances, as well as coupling due to decomposition errors. Smooth boundary layer implementation of the controller is examined and quantified for the given isolation requirement. The effects of geophone dynamics and mode combination are also explored. Simulation results verifying the design are presented in Section 4. The experiment verification of our algorithm of frequency-shaped manifolds for vibration isolation and its adaptive version [16] is briefly presented in Section 5, which also generalizes the design of frequency-shaped sliding surfaces from the point of view of linear compensator design and of contraction theory. This allows linear or nonlinear target dynamics of the

same order as the nominal plant to be systematically specified. Concluding remarks are given in Section 6.

2. Modal decomposition and experimental modal analysis

Fig. 1 shows a typical configuration of a multi-dof isolation system. A two-dof system is shown there, but it can be up to six dof. A multi-dof isolation table is supported on the ground by springs and dampers. On the isolation table are the other stages (passive or active), or payload. The measurements are the displacements relative to the floor and the absolute velocities of the table. (A geophone senor produces a signal proportional to the absolute velocity above its natural frequency.) The control forces can be generated by linear voice-coil motors, pneumatic or hydraulic actuators, or piezoelectric stacks. Our goal is to design the controller to achieve the vibration attenuation of the floor excitation under plant uncertainties and disturbances from the upper stages and payload. The performances of isolation systems are often specified in the frequency domain, such as the precision machine tools [17], gravitational wave detectors [14], and micro-gravity experiments [12].

2.1. Modal decomposition

The mass, stiffness and damping properties of the isolation system can be obtained from mechanical design, and an analytical or finite-element model can be constructed. However, in practice it is hard to model the dynamics of the system accurately (even for the first stage) because of the uncertainties on the joints, contacts, damping, flexural modes, and payload. It is well known that the mathematical model often does not match the experimental measurements and cannot be used in MIMO controller design with confidence. Bode/Nyqusit-based approaches have been extended to MIMO systems somehow (see the text by Hung and MacFarlane [18]), but the results are not convenient for use in controller synthesis. A great deal of efforts has been invested in model development, such as system identification from experimental observation [19], and model updating [20], which tries to correct the finite element models using the test data. In the past 40 years, experimental modal analysis [21] has been developed as an important and powerful tool in structural dynamics. In the following, we show how to use modal testing techniques to identify

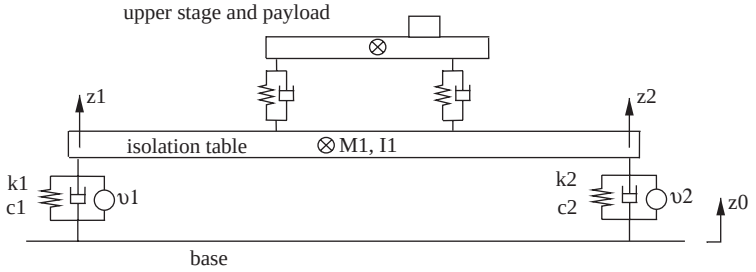

Fig. 1. Typical configuration of a multi-dof isolation system.

the modal frequencies, damping, and mode shapes for the isolation system, and then use them in the controller design.

The governing equation of the n-dof isolation table with n force actuators takes the form

$$M\ddot{z} + C(\dot{z} - \dot{z}_0) + K(z - z_0) = B_v v + f_d, \tag{1}$$

where M, C, and K are, respectively, the mass, damping, and stiffness matrices of dimension $n \times n$, B_v is an $n \times n$ matrix taking into account the effect of actuator locations, f_d is the vector of disturbance forces acting on the isolation table, such as external forces or dynamics of the upper stages and payload, and z_0 is the vector of floor displacements.

Since the mass matrix M is nonsingular, Eq. (1) is identical to

$$\ddot{z} + M^{-1}C(\dot{z} - \dot{z}_0) + M^{-1}K(z - z_0) = M^{-1}B_v v + M^{-1}f_d. \tag{2}$$

The matrix $M^{-1}K$ can usually be written in the diagonalized form:

$$M^{-1}K = V\Lambda V^{-1}, \tag{3}$$

where Λ is a diagonal matrix composed of ω_i^2, $i = 1, 2, \ldots n$, ω_i is the undamped *modal frequency*, and the matrix V is composed of the *mode shape* vectors.

Take the transformation

$$x = V^{-1}z \quad \text{and} \quad u = V^{-1}M^{-1}B_v v = Wv. \tag{4}$$

Then, in modal coordinates we have

$$\ddot{x} + V^{-1}M^{-1}CV(\dot{x} - \dot{x}_0) + \Lambda(x - x_0) = u + V^{-1}M^{-1}f_d, \tag{5}$$

where $V^{-1}M^{-1}CV$ is the diagonal in the case of proportional damping $C = \alpha M + \beta K$ (α and β are constants). The ith diagonal item of $V^{-1}M^{-1}CV$ is $2\zeta_i\omega_i$, where ζ_i is the so-called *modal damping ratio*. Let us denote the irth off-diagonal entry as ε_{ir}, and ith element of vector $V^{-1}M^{-1}f_d$ as d_i; then we have

$$\ddot{x}_i + 2\zeta_i\omega_i(\dot{x}_i - \dot{x}_{0i}) + \omega_i^2(x_i - x_{0i}) = u_i + d_i - \sum_{r=1, r\neq i}^{n} \varepsilon_{ir}(\dot{x}_r - \dot{x}_{0r}), \quad i = 1, 2, \ldots n. \tag{6}$$

2.2. Experimental modal analysis

By using the modal transformation (4), the governing equation (1) of $2n$th order has been decomposed as n second-order systems in modal coordinates. There are two advantages of this modal decomposition. The first is that a MIMO control of a high-order system has been changed into lower-order SISO problems, which can be handled more easily. These lower-order SISO problems also have clear physical meaning: we can design each loop to control the individual mode. The second advantage is that the matrices V and W used in the decomposition and the parameters ζ_i and ω_i can be obtained from experimental modal testing. In modal testing [21], the matrix B_v is usually taken as identity. The idea for general case of B_v is similar.

Let us first assume proportional damping. From Eqs. (1) and (4), we obtain the forced response from $v(\mathrm{j}\omega)$ to $z(\mathrm{j}\omega)$ (without z_0 and f_d) as

$$\left[\ \omega_i^2 + 2\mathrm{j}\zeta_i\omega\omega_i - \omega^2\ \right] V^{-1}z(\mathrm{j}\omega) = V^{-1}M^{-1}B_v v(\mathrm{j}\omega) = Wv(\mathrm{j}\omega),$$

where $\left[\ \cdot\ \right]$ is a diagonal matrix. That is, the frequency response function (FRF) matrix $v(j\omega) \to z(j\omega)$ takes the form

$$H(j\omega) = V\left[\ \omega_i^2 + 2j\zeta_i\omega\omega_i - \omega^2\ \right]^{-1} W = \sum_{i=1}^{n} \frac{V_i W_i^{\mathrm{T}}}{\omega_i^2 + 2j\zeta_i\omega\omega_i - \omega^2}, \tag{7}$$

where V_i is the ith mode shape (ith column of V), and W_i is the ith column of W, which represents the contribution of input v_i to the responses. (Therefore, W is called the *mode participation* matrix.)

Eq. (7) is the central relationship upon which the modal testing techniques are based. Using modal testing devices, or directly using the actuators and sensors of the isolation system, we can measure the FRF matrix. Then, we can use curve fitting to extract the mode shape vectors V_i, modal participation vectors W_i, modal frequencies ω_i, and modal damping ζ_i, where $i = 1, 2, \ldots, n$. From Eq. (7), we see that the residue matrix $V_i W_i^T$ at each mode is a rank-one matrix; therefore, theoretically all the modal parameters can be extracted from any column and any row of the FRF matrix. Specially, if all the actuators and sensors are of collocated pairs, the FRF matrix will be symmetric, and W can be taken as V^{-1}. (Because of scaling effects, WV might not be the identity matrix, but WV is diagonal.) Multi-input multi-output modal analysis has also been proposed for large-scale structures in case some mode cannot be excited or observed. In the past 20 years, different time-domain and frequency-domain fitting methods have been developed, and software packages are also available, such as MODENT Suite^{TM} by ICATS Company and STAR System^{TM} by Spectral Dynamics, Inc.

Proportional damping is a good approximation for most engineering structures which are lightly damped. For nonproportional damping, similar relationships as Eq. (7) exist, but the mode shapes are generally complex-valued vectors. The undamped eigenvectors are not the damped eigenvector any more, since the nonproportionally damped modes are not simply in the pattern of in-phase and out-of-phase.

In the foregoing analysis, we assume that the number of actuators and the number of measurements is equal to the degrees of system. This is a so-called *complete modal model*, which is convenient for theoretical study. In structure control, we might only be concerned with the first m modes by using m actuators and sensors. For this type of *incomplete modal model*, the foregoing procedure is still valid by replacing the inverse of modal shape matrix V and modal participation matrix W in the transformation (4) with the pseudo-inverse of size $m \times n$. But some attention should be paid to the effect of performance-reducing control spillover and destabilizing observation spillover (see, e.g., Refs. [22–24]).

Other than experimental modal analysis, the decomposition matrices may also be obtained from the measured FRF matrix by using an optimal decoupling procedure developed in Ref. [25] based on Owens' theory of dyadic systems [26].

3. Sliding control for frequency-domain performance

With the modal transformation (4) in Section 2, we can transform a MIMO high-order isolation problem into second-order SISO control, and all the parameters ω_i, ζ_i, V, and W used in

the modelling and decomposition can be obtained from experimental or theoretical modal analysis. Hence, we can design each SISO controller for the individual mode to achieve the isolation performance, as shown in Fig. 2.

Rewrite the governing equation in modal coordinate as

$$\ddot{x}_i + 2\zeta_i\omega_i(\dot{x}_i - \dot{x}_{0i}) + \omega_i^2(x_i - x_{0i}) = u_i + d_i - \sum_{r=1, r\neq i}^{n} \varepsilon_{ir}(\dot{x}_r - \dot{x}_{0r}), \quad i = 1, 2, \ldots, n. \tag{8}$$

We can find, however, that the modes are not completely decoupled because of the coupling by nonproportional damping. Another question is that there are uncertainties in the natural frequency frequencies ω_i and damping ζ_i due to the modal testing error or time-varying of structures. Third, the system is subjected to payload disturbance or upper stage dynamics other than unknown base excitation. It is feasible to design a linear controller to achieve some performance of vibration isolation and disturbance rejection, for example, using absolute velocity or acceleration feedback. However, since there lack true inertia sensors, due to the sensor dynamics at low frequency, such a feedback generally results in a crossover at low frequency in addition to the crossover at high frequency (see Ref. [27], for example). This low-frequency crossover will limit the feedback gain and cannot achieve a steep enough vibration rolloff in the frequency domain. Positive feedback of relative position can directly decrease the resonant frequency ω_i and attenuate the vibration, but such a cancellation of stiffness may make the system unstable under the uncertainties. Therefore, we turn to sliding control, one of the main robust control techniques for dealing with model uncertainties and external disturbance [28–30].

3.1. Sliding control and frequency-domain performance

Sliding control is based on the idea of transforming an original control problem into one of driving system dynamics onto a specific manifold in the state space. In essence, it replaces a possibly high-order problem by a first-order problem, that of controlling the "distance" to the manifold to zero. As a nonlinear control method, sliding control has been mainly used in tracking control problems (see e.g., Ref. [28]). For vibration isolation/suspension, however, our main concern is frequency-domain performance. In this context, an idea [10–12] is to choose a so-called reference plant according to the performance requirement, then control the real plant to track the

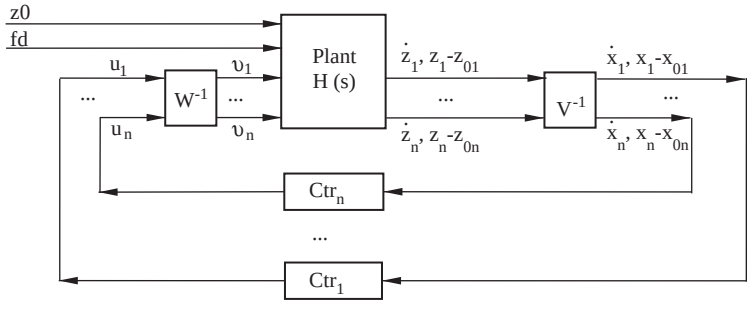

Fig. 2. Modal control of a multi-dof isolation system.

states or certain outputs of the reference plant. This, however, has three shortcomings. One is that it usually requires the measurement of ground vibration, which is not practical in many cases, such as for vehicle suspension systems. Another is the tradeoff of bandwidth: a wide bandwidth decreases tracking error but it can increase control activity or chattering. Third, the performance during the transient stage cannot be guaranteed. In the following, rather than defining and tracking a reference model, we directly design the sliding surface to meet the requirement of frequency-domain performance. This approach does not have the foregoing shortcomings of a reference-tracking schedule.

For the ith mode of the isolation system in second-order form (8), the measured variables are often $x_i - x_{i0}$ and $\dot{x}_i$. The conventional sliding variable can be defined as

$$\sigma_i = \lambda_i(x_i - x_{i0}) + \dot{x}_i, \tag{9}$$

where λ_i is a constant. Then, on the sliding surface $\sigma_i = 0$, the system dynamics are

$$\frac{x_i(s)}{x_{i0}(s)} = \frac{\lambda_i}{s + \lambda_i}, \tag{10}$$

where s is the Laplace operator. That is, the base vibration is attenuated at -20 dB/decate above the frequency λ_i. However, for the second-order plant (8), the such vibration attenuation -20 dB/decate as a first-order system attained by using the conventional sliding control might be not fast enough.

Instead of designing the sliding surface as the intersection of the hyperplanes defined in the plant states, we can replace λ_i as a linear operator $L_i(s)$. This is

$$\sigma_i = L_i(s)(x_i - x_{i0}) + \dot{x}_i. \tag{11}$$

Then, once the system is driven to the sliding surface $\sigma_i = 0$, the dynamics become

$$\frac{x_i(s)}{x_{i0}(s)} = \frac{L_i(s)}{s + L_i(s)}. \tag{12}$$

For example, we can take $L_i(s) = (b_1 s + b_0)/(s + a_0)$. Then

$$\sigma_i = \frac{b_1 s + b_0}{s + a_0}(x_i - x_{i0}) + \dot{x}_i. \tag{13}$$

Also, on this sliding surface we have

$$\frac{x_i(s)}{x_{i0}(s)} = \frac{b_1 s + b_0}{s^2 + (a_0 + b_1)s + b_0}. \tag{14}$$

Thus, we achieve a second-order dynamics for the second-order plant (8) by using the sliding surface (13).

The idea of taking the sliding surface as a manifold defined by linear operators was originally proposed by Young and Ozguner [15] for the purpose of reducing the effect of unmodeled high-frequency dynamics in flexible manipulators. Therein, it has been interpreted as a low-pass filter and given the name "frequency-shaped sliding surface". A similar strategy, called dynamic sliding mode, has also been proposed by Chan and Gao [31] and Yao and Tomizuka [32] for robot manipulator control. In the following, we provide a physical interpretation of the frequency-shaped sliding surface as applied to vibration isolation.

3.2. Physical interpretation: skyhook

Let us assume $b_1 = 0$ in the frequency-shaped sliding surface (8), then the ideal dynamics (on the sliding surface) are

$$\frac{x_i(s)}{x_{i0}(s)} = \frac{b_0}{s^2 + a_0 s + b_0}. \tag{15}$$

The mechanical system corresponding to this transmission is shown in Fig. 3(a), where a unit mass is supported on the vibrating base via a spring of stiffness b_0 and is connected to the inertial sky via a dashpot of damping coefficient a_0. This is exactly the skyhook damping suggested by Karnopp [1,2].

Usually the dashpot can only connect to the base since there is no practical inertial sky. Fig. 3(b) shows such a configuration. And the corresponding transmission from x_{i0} to x_i is

$$\frac{x_i(s)}{x_{i0}(s)} = \frac{a_0 s + b_0}{s^2 + a_0 s + b_0}. \tag{16}$$

To highlight the advantage of skyhook damping yielded by the frequency-shaped sliding surface, Fig. 4 compares the vibration transmissions in the frequency domain for the two configurations in Fig. 3. We can see that (1) there exists tradeoff of damping in the classical configuration between the high-frequency and low-frequency performances: larger damping yields smaller peak at resonant frequency but impairs the vibration attenuation at high frequency; (2) there is no such conflict in the skyhook; (3) skyhook is an ideal configuration of vibration isolation, much better than the classical configuration (b). The skyhook configuration also eliminates the tradeoff between rejection of disturbances directly acting at the payload and isolation from ground vibration. This is why the skyhook damper has become an important concept in vibration isolation and has been an effective target in many isolation systems [10,11,3].

The choice of $L_i(s) = b_0/(s + a_0)$ yields the ideal skyhook effect. Similarly, we can also design the frequency-shaped sliding surface to achieve a faster vibration attenuation in the frequency domain at the payment of high control authority. A more general approach for selection of $L_i(s)$ is given in Section 5.

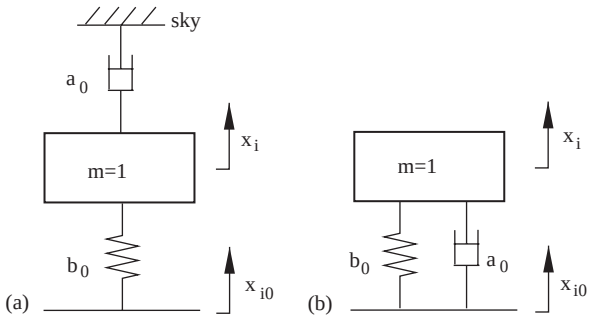

Fig. 3. (a) Skyhook configuration, (b) the classical configuration.

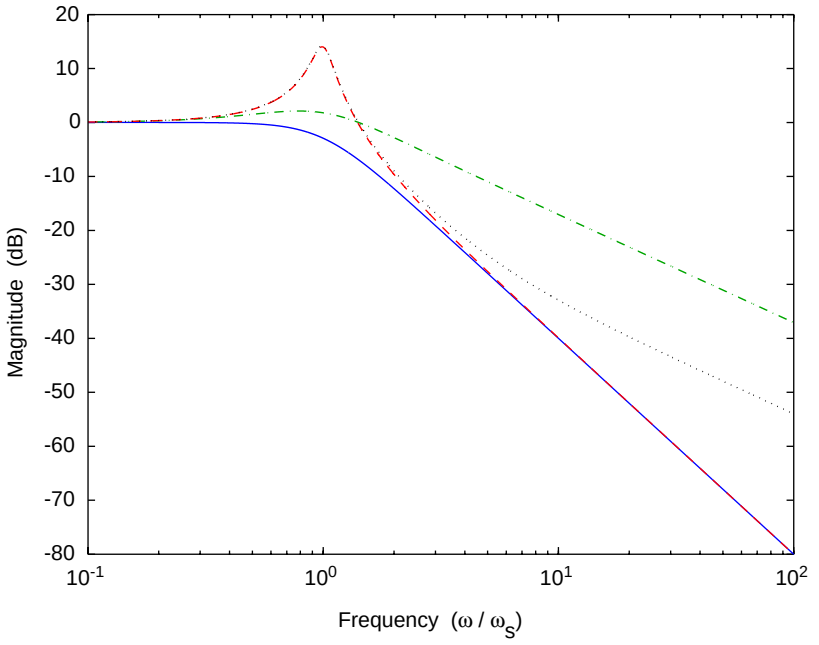

Fig. 4. Vibration responses of the two configurations ($a_0 = 2\zeta_s\omega_s, b_0 = \omega_s^2$). Skyhook with $\zeta_s = 0.7$ (solid), skyhook with $\zeta_s = 0.1$ (dash), classical with $\zeta_s = 0.7$ (dash-dot), classical with $\zeta_s = 0.1$ (dot).

3.3. Switching control for vibration isolation

We have just seen that the ideal isolation performance is achievable once the dynamics of the system is driven to the sliding surface. We now derive the corresponding switching control law for this purpose, in a manner similar to Ref. [33].

From the choice of sliding surface,

$$\sigma_i = L_i(s)(x_i - x_{i0}) + \dot{x}_i,$$

we obtain

$$\dot{\sigma}_i = sL_i(s)(x_i - x_{i0}) + \ddot{x}_i. \tag{17}$$

Combining with the plant model (8), we can obtain the best approximation $\hat{u}_i$ of the continuous control law that achieves $\dot{\sigma}_i = 0$:

$$\hat{u}_i = [\hat{\omega}_i{}^2 - sL_i(s)](x_i - x_{i0}) + 2\hat{\zeta}_i\hat{\omega}_i(\dot{x}_i - \dot{x}_{i0}) + \sum_{r=1, r\neq i}^{n} \hat{\varepsilon}_{ir}(\dot{x}_r - \dot{x}_{0r}) - \hat{d}_i, \tag{18}$$

where $\hat{\omega}_i$, $\hat{\zeta}_i$, $\hat{\varepsilon}_{ir}$, and $\hat{d}_i$ are, respectively, the estimations of the ith modal frequency, ith modal damping, irth entry of the damping matrix, and the external disturbance on ith mode. Note that $\hat{\omega}_i$ and $\hat{\zeta}_i$ can be obtained from experimental modal analysis, $\hat{\varepsilon}_{ir}$ and $\hat{d}_i$ can often be taken as zero.

Eq. (18) is the ideal (linear) control force for the nominal plant to achieve skyhook isolation. To ensure that the actual plant dynamics reach the sliding surface in finite time despite the model uncertainties and external force, a discontinuous term is added to control force u_i:

$$u_i = \hat{u}_i - k_i \operatorname{sgn}(\sigma_i). \tag{19}$$

The sliding condition is the same as that in the standard sliding control [28]:

$$\frac{1}{2}\frac{\mathrm{d}}{\mathrm{d}t}\sigma_i^2 \leqslant -\eta_i|\sigma_i|. \tag{20}$$

To guarantee this condition, we have to select k_i large enough:

$$\begin{aligned} k_i = \eta_i &+ |\omega_i^2 - \hat{\omega}_i^2|_{\max}|x_i - x_{i0}| + 2|\zeta_i\omega_i - \hat{\zeta}_i\hat{\omega}_i|_{\max}|\dot{x}_i - \dot{x}_{i0}| \\ &+ \sum_{r=1, r\neq i}^{n} |\varepsilon_{ir} - \hat{\varepsilon}_{ir}|_{\max}|\dot{x}_r - \dot{x}_{0r}| + |d_i - \hat{d}_i|_{\max}, \end{aligned} \tag{21}$$

where the bound of ω_i and ζ_i can be obtained practically, and ε_{ir} is generally less than or equal to the ith diagonal term $2\hat{\zeta}_i\hat{\omega}_i$ of the damping matrix. The upper bound of $|d_i - \hat{d}_i|$ often cannot be obtained so directly in practice. We write

$$d = V^{-1}M^{-1}f_d = V^{-1}M^{-1}VV^{-1}f_d = \begin{bmatrix} \ddots & & \\ & 1/m_i & \\ & & \ddots \end{bmatrix} V^{-1}f_d,$$

where the modal mass m_i can be obtained from experimental modal analysis. The bound of f_d depends on the intensity of ground excitation and the properties of payloads or upper stages. We assume

$$|f_{di}| = |f_{di}(t, \dot{z}, z, \dot{z}_0, z_0)| \leqslant \Psi_{0i}(t) + \Psi_{1i}(t)\,\|\,[\dot{z}^{\mathrm{T}}, (z - z_0)^{\mathrm{T}}]^{\mathrm{T}}\,\|, \tag{22}$$

where Ψ_{0i} and Ψ_{1i} are some constants and $i = 1, 2, \ldots, n$. Since we usually have some a priori knowledge about the intensity of ground excitation and the upper payloads, we can often estimate a constant upper bound as Ψ_{0i} and take $\Psi_{1i} = 0$. This requirement of a priori knowledge of upper bounds of disturbances in sliding control may be relaxed by using disturbance observers (see, e.g., Refs. [9,34]).

In isolation systems, the variables available are $z - z_0$, $\dot{z}$ and $\dot{z}_0$, which may be measured with displacement sensors and geophones. Hence we can obtain $x - x_0$ and $\dot{x} - \dot{x}_0$ for switching control (11), (18), (19), and (21). And the controller force v can be constructed as $v = W^{-1}u$. In cases (for economic consideration) where we do not have geophone sensors on the ground, we can use $(s/(1 + \tau_i s))(x_i - x_{i0})$ as an estimation of $\dot{x} - \dot{x}_0$. Such an estimation will not create trouble in practice because the spectrum density of floor excitation only distributes in low-frequency bandwidth [17].

3.4. Boundary layer analysis and continuous control

In sliding control, chattering is one of the main concerns. Although frequency-shaped sliding control has the advantage of reducing the excitation of high-frequency unmodeled dynamics, the robustness to chattering is only implicitly addressed [30]. In the following, we will make a smooth approximation of the switching control law by choosing a proper boundary layer, in a manner similar to Ref. [33].

Consider a constant boundary layer thickness of Φ_m. Outside the boundary layer the system dynamics are the same as the switching control. Inside the boundary layer,

$$\sigma_i(t) = L_i(s)(x_i - x_{i0}) + \dot{x}_i = \Phi_i(t) \leqslant \Phi_m. \tag{23}$$

Then,

$$x_i(t) = \frac{L_i(s)}{s + L_i(s)} x_{i0}(t) + \frac{1}{s + L_i(s)} \Phi_i(t). \tag{24}$$

Hence, after transients, the displacement error due to the boundary layer interpolation is bounded by

$$|e_{x_i}(t)|_\Phi = \left| \int_0^t h(\tau)\Phi_i(t-\tau)\,\mathrm{d}\tau \right| \leqslant \Phi_m \int_0^\infty |h(\tau)|\,\mathrm{d}\tau = \Phi_m \|h(t)\|_1, \tag{25}$$

where $h(t)$ is the impulse response of $1/(s + L_i(s))$.

In particular, choosing $L_i(s) = b_0/(s + a_0)$ for the skyhook effect, inside the boundary layer we have

$$x_i(t) = \frac{b_0}{s^2 + a_0 s + b_0} x_{0i}(t) + \frac{s + a_0}{s^2 + a_0 s + b_0} \Phi_i(t). \tag{26}$$

3.5. Discussion

In the foregoing parts of this section, we assumed that the absolute velocity can be measured perfectly, but in practice the velocity measurement is only valid above some frequency. For a geophone sensor the relation of measured signal $\hat{\dot{x}}_i$ and the velocity $\dot{x}_i$ generally takes the form

$$\hat{\dot{x}}_i = \frac{s^2}{s^2 + 2\zeta_g \omega_g s + \omega_g^2} \dot{x}_i, \tag{27}$$

where ω_g and ζ_g are the resonant frequency and damping ratio of the geophone sensor. With the measurement $\hat{\dot{x}}_i$, the actual sliding surface for $L_i(s) = b_0/(s + a_0)$ becomes

$$\hat{\sigma}_i = \frac{b_0}{s + a_0}(x_i - x_{i0}) + \hat{\dot{x}}_i \tag{28}$$

and the achieved dynamics $x_{i0} \to x_i$ on the sliding surface $\hat{\sigma}_i = 0$ becomes

$$\frac{x_i(s)}{x_{i0}(s)} = \frac{b_0(s^2 + 2\zeta_g \omega_g s + \omega_g^2)}{s^4 + a_0 s^3 + b_0(s^2 + 2\zeta_g \omega_g s + \omega_g^2)}. \tag{29}$$

Using the Routh–Hurwitz criterion, the stability of Eq. (29) is ensured if

$$\frac{\omega_s}{\omega_g} > \frac{\zeta_s}{\zeta_g} + \frac{\zeta_g}{\zeta_s}, \tag{30}$$

where ω_s and ζ_s are the resonant frequency and damping ratio of the ideal skyhook isolator ($\omega_s = \sqrt{b_0}$, and $\zeta_s = a_0/2\sqrt{b_0}$). If we choose the damping ratio ζ_s of the ideal skyhook isolator close to ζ_g of the geophone, then the geophone resonant frequency should be smaller than half of the resonant frequency of the ideal skyhook isolator. If the geophone resonance is very low ($\omega_g/\omega_s \ll 1$), then the ideal skyhook effect can be closely attained.

By designing dynamic sliding surfaces, we can directly achieve the skyhook effect for each mode of vibration. The entire performance of the multi-mode system is the combination of the individual modes. Suppose that the target dynamics (skyhook) of the ith mode is $x_i(s)/x_{i0}(s) = T_{x_i/x_{i0}}(s)$. From the modal transformation (4), we find that on the sliding surface the entire performance is

$$z(s) = V[\ T_{x_i/x_{i0}}(s)\ ]V^{-1}z_0(s). \tag{31}$$

Specifically, as an example, if the target of each mode is chosen to be identical, $T_{x_i/x_{i0}} = T_{x/x_0}(s)$, $i = 1, 2, \ldots, n$, then $z_i(s) = T_{x/x_0}(s)z_{i0}(s)$. If the isolation requirement is stated as a frequency-domain envelope in natural coordinates $z_{i0}(s) \to z_i(s)$, we can use the relation of Eq. (31) to obtain the skyhook targets $T_{x_i/x_{i0}}(s)$ in modal coordinates.

In practice, identification errors also exist in the mode shape matrix V and participation matrix W. This yields mode coupling even in proportionally damped systems. To explicitly take the effect of V and W errors into account in the framework of sliding control is challenging. Practically, we may check that the $W^{-1}H(j\omega)V^{-1}$ is diagonally dominant before we use matrices V and W in controller design. In addition, the effect of some modal coupling can be reduced implicitly by encompassing it as a part of disturbance d_i. Successful applications of experiment-based modal control have been reported, e.g., Refs. [6,35], yet the accurate identification of the modal shape matrix V and participation matrix W is still an important research topic.

4. Simulation results

In this section, we take a two-dof vibration isolator as an example and demonstrate that the skyhook effect can be robustly achieved using modal decomposition and frequency-shaped sliding control.

As shown in Fig. 1, the two-dof isolation table used in simulation has a mass 500 kg and rotational inertia 250 kg m^2. The distances from the center of mass to mounting 1 and mounting 2 are 1.0 and 1.4 m, respectively, and $k_1 = k_2 = 3 \times 10^5$ N/m, $c_1 = 200$ N s/m, $c_2 = 120$ N s/m. Suppose we identify modal frequencies ω_1 as 5.4 ± 0.1 Hz and ω_2 as 9.5 ± 0.1 Hz, and modal damping $2\zeta_1\omega_1$ as 0.7 ± 0.2 and $2\zeta_2\omega_2$ as 1.7 ± 0.3, and the mode shape as

$$V = \begin{bmatrix} -1.0 & -0.6 \\ -0.6 & 1.0 \end{bmatrix}.$$

The upper bound of off-diagonal damping in modal coordinates is taken as $\min(2\hat{\zeta}_1\hat{\omega}_1, 2\hat{\zeta}_2\hat{\omega}_2) = 0.7$.

The dynamics of upper stages/payload may be unknown or changeable. As discussed in Section 2, their effect can be considered as a disturbance force vector f_d. We assume that the bound of $|f_d|$ could be obtained as

$$|f_d| \leqslant \begin{bmatrix} 20 \\ 20 \end{bmatrix} + \begin{bmatrix} 2 \times 10^4 \\ 1 \times 10^4 \end{bmatrix} (|\dot{z}_1| + |\dot{z}_2|).$$

In this simulation, the upper stage/payload is taken as a two-dof system supported symmetrically on the isolation table with a pair of spring-dashpots of 1500 N/m and 8 N s/m. Its mass is 125 kg (25% of the isolated table), and rotational inertia is 10 kg m^2. The distance between the spring-dashpot connections is 1.0 m, and the mass center of the upper stage is located above the geometric center of the isolation table.

The target dynamics z_1/z_0 and z_2/z_0 are chosen as skyhook of frequency 0.1 Hz and damping ratio 0.7. Fig. 5 shows the transmission from $z_0 \to z_1$ and $z_0 \to z_2$ of the plant and the skyhook target. The resonant frequencies of the actual plant (eighth order) are 0.778, 1.378, 5.415, and 9.555 Hz. And the nominal plant is in fourth order.

We design the controller using modal decomposition and a frequency-shaped sliding surface in which we take $\eta_1 = \eta_2 = 0.2$. Fig. 6 shows the responses $z_1(t)$ of the system at zero initial conditions with and without control under harmonic ground excitation $z_0 = 0.001 \sin(1.38 \times 2\pi t)$ m, $t \geqslant 0$. We see that the vibration of the isolation table is greatly attenuated.

Figs. 7 and 8 show the responses of $z_1(t)$ and $z_2(t)$ with switching control compared with the ideal outputs of the skyhook system excited at resonant frequencies 1.38 Hz ($z_0 = 0.001 \sin(1.38 \times 2\pi t)$ m) and 9.55 Hz($z_0 = 0.001 \sin(9.55 \times 2\pi t)$ m), respectively.

From these figures, we can see that the ideal skyhook effect is attained under the uncertainties and disturbance. The control forces v_1 and v_2 of switching control are shown in Fig. 9.

To reduce the chattering of control forces, we design a continuous controller using the boundary layer. We take the boundary thickness Φ_m as $5 \times 10^{-6}/\|h(t)\|_1$ (see Eq. (25)) and replace $\mathrm{sgn}(\sigma_i)$ in Eq. (19) with a saturation interpolation $\mathrm{sat}(\sigma_i/\Phi_m)$. Fig. 10 shows the errors of the response $z_1(t)$ and $z_2(t)$ in comparison with the ideal output of the skyhook system.

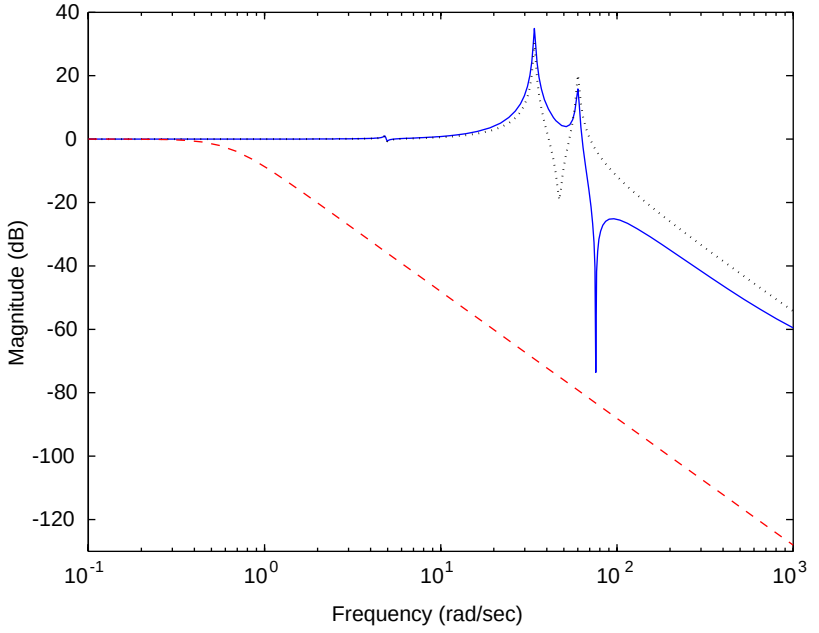

Fig. 5. Transmission of uncontrolled plant and target dynamics: uncontrolled z_1/z_0 (solid), uncontrolled z_2/z_0 (dot), skyhook target (dash).

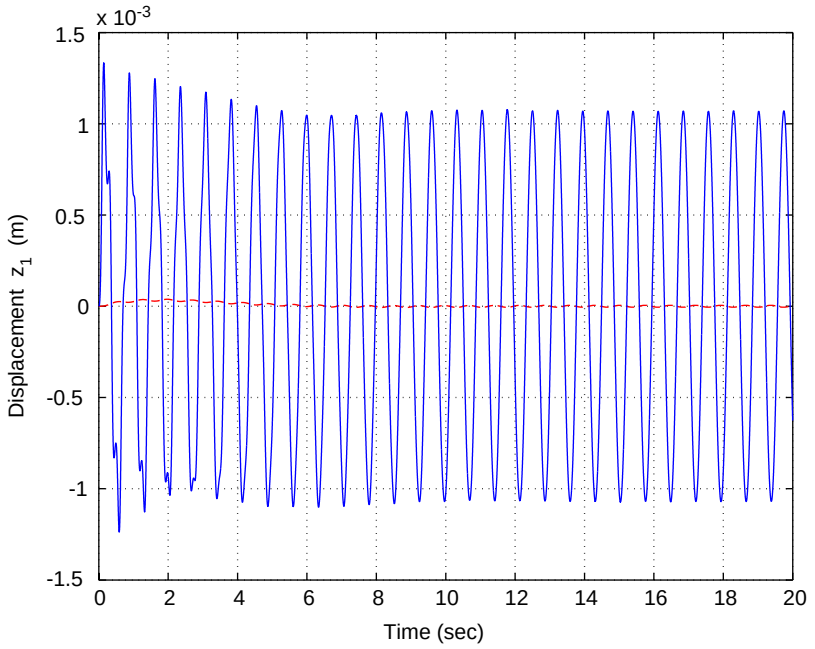

Fig. 6. Responses of $z_1(t)$ with switching control (dash) and without control (solid).

We see that the peak error due to a boundary layer is less than $\Phi_m\|h(t)\|_1 = 5\,\mu\text{m}$. The continuous control forces v_1 and v_2 are shown in Fig. 11. Comparing Figs. 11 and 9, we see that the chattering has been reduced.

In Figs. 10 and 11, the errors due to boundary layer is one order smaller than the expected values, and the control forces are still not very smooth. The reason is that the constant k_i in "$k_i\,\text{sat}(\sigma_i/\Phi_m)$" is over-estimated, such that the actual boundary layer thickness is much thinner than the expected one. By taking the boundary layer as Φ_m as $1 \times 10^{-4}/\|h(t)\|_1$, Fig. 12 shows the corresponding errors of displacements due to this boundary layer, and Fig. 13 shows the corresponding control forces v_1 and v_2 under ground excitation $z_0 = 0.001\,\sin(1.38 \times 2\pi t)\,\text{m}$. We see that these control forces are much more smooth than before.

Note that simulation results in Figs. 7 and 8 show that the controlled system approaches the skyhook target from the beginning. The displacement errors in Figs. 10 and 12 also show that there is no obvious "transition" stage. This is not by chance if we consider the following two reasons. First, the target dynamics is achieved once the system is driven to the sliding surface, while in the schedule of reference tracking (see Refs. [10–12]) there are still error dynamics (low-pass filter) between the controlled system and the target on the sliding surface. Second, the additional states in the frequency-shaped sliding surface (states in $L_i(s)$) offer the feasibility to choose the initial states, such that the dynamics of controlled system starts on the sliding surface $\sigma_i = 0$ at the beginning $t = 0$, and therefore, the transient performance is guaranteed. This guarantee of transient performance is the third advantage of the frequency-shaped sliding surface over the conventional sliding control and reference tacking schedule.

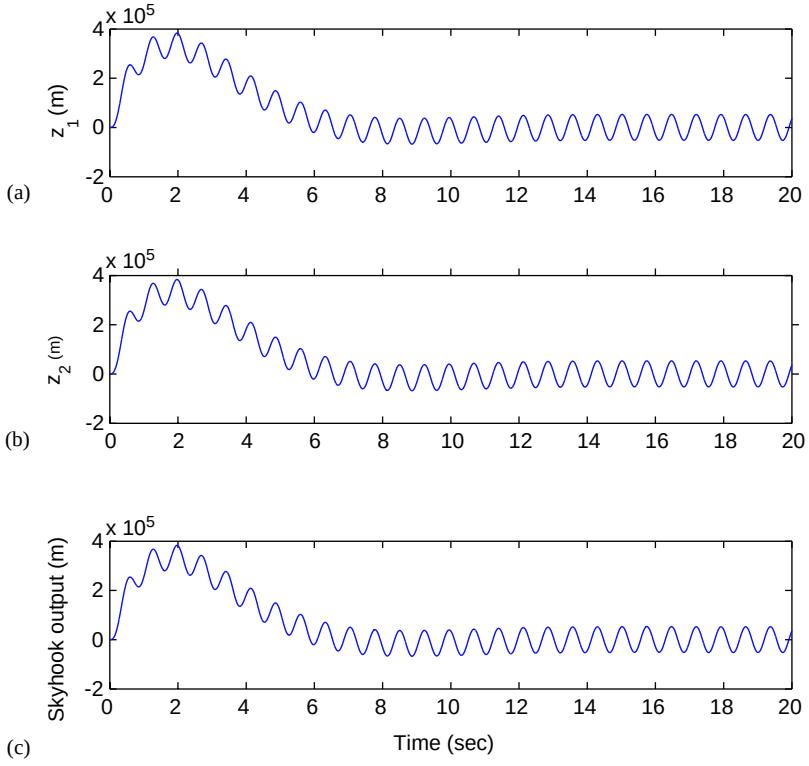

Fig. 7. Responses of the controlled system and skyhook system under ground excitation $z_0 = 0.001 \sin(1.38 \times 2\pi t)$ m: (a) $z_1(t)$, (b) $z_2(t)$, (c) skyhook target.

5. Extensions and experiment verification

In this section, we will discuss the design of sliding surface from the view of feedback–feedforward control and contraction theory, then extend the sliding control to modal reaching adaptive control for vibration isolation. Experimental verifications of sliding and adaptive isolation are also reported.

5.1. Sliding surface and input–output system

Simulation results in the previous section show that the ideal skyhook effect of isolation can be robustly attained with the frequency-shaped sliding control and modal decomposition. The procedure of designing the sliding surface in Section 3, or equivalently the choice of $L_i(s)$, is essentially pole and zero assignment. For example, we set $b_1 = 0$ in Eq. (13) to put the zero at infinity, and chose a_0 and b_0 for the desired damping ratio and natural frequency of skyhook isolation. Though the SISO system is determined uniquely by pole, zero and gain, it is more general (e.g., extension to MIMO sliding) and more convenient to examine the input–output relation therein.

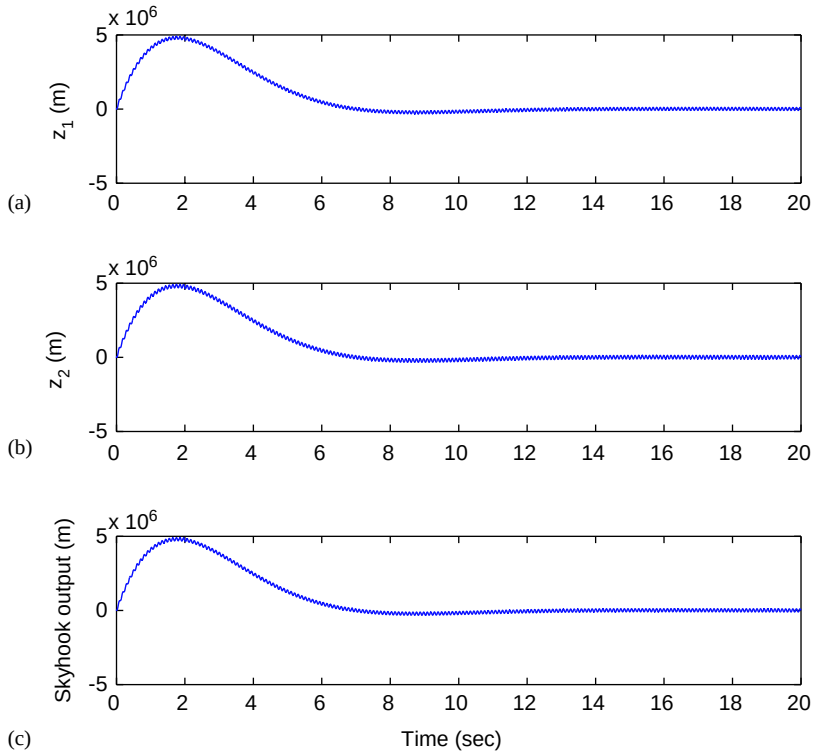

Fig. 8. Responses of the controlled system and skyhook system under ground excitation $z_0 = 0.001 \sin(9.55 \times 2\pi t)$ m: (a) $z_1(t)$, (b) $z_2(t)$, (c) skyhook target.

Eq. (24) shows the system dynamics of $x_i(t)$ under the excitations $x_{i0}(t)$ and $\Phi_i(t)$ (inside boundary layer $\Phi_i(t) = \sigma_i(t)$). Let us rewrite Eq. (24) as

$$x_i(t) = \frac{(1/s)L_i(s)}{1 + (1/s)L_i(s)}\, x_{i0}(t) + \frac{(1/s)}{1 + (1/s)L_i(s)}\, \Phi_i(t). \tag{32}$$

The block diagram of the system described by the above equation is shown in Fig. 14.

We see that the sliding surface in fact defines a control system: plant $(1/s)$, controller $L_i(s)$, inputs $x_{i0}(t)$ and $\Phi_i(t)$. This system is very common to control engineers, and thus, we can design the sliding surface $L_i(s)$ using the classical LTI control methodologies according to the performance specifications. We can also write it in the form of linear fractional transformation as shown in Fig. 15, where the generalized plant is given by

$$P(s) = \begin{bmatrix} 1/s & 0 & 1/s \\ -1/s & 1 & -1/s \end{bmatrix}.$$

Thus, we can also use state-space LTI control techniques, such as H_2/LQG, H_∞, or $\mathscr{L}_1$, to design the sliding surface. In addition, the spectrum of the ground noise can also be taken into account if we include a shape filter of x_{i0} in the generalized plant.

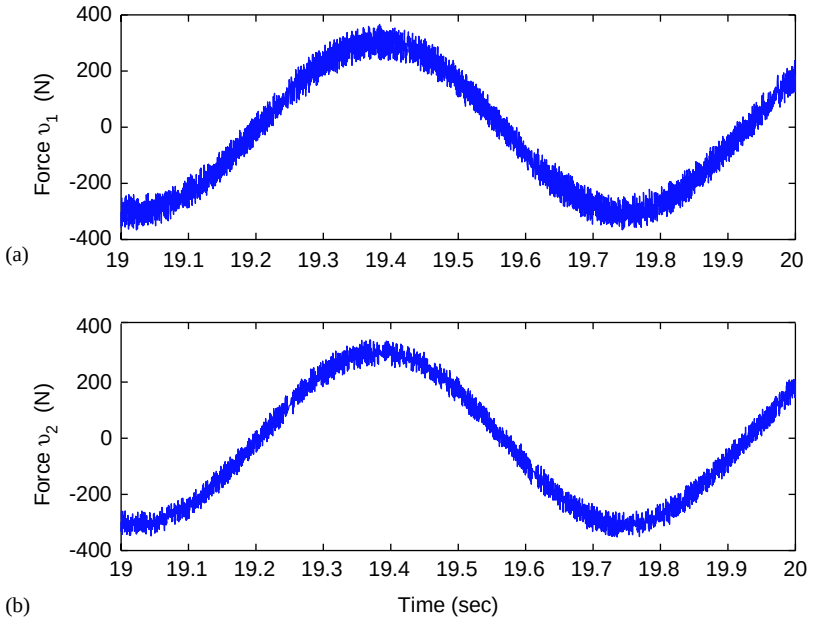

Fig. 9. Control forces with switching control under ground excitation $z_0 = 0.001 \sin(1.38 \times 2\pi t)$ m: (a) force $v_1(t)$, (b) force $v_2(t)$.

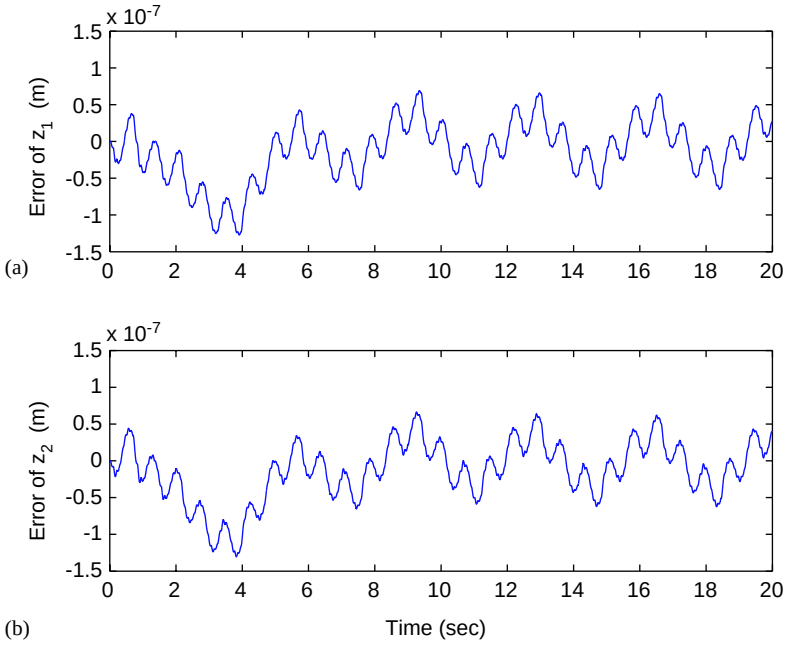

Fig. 10. Displacement errors due to boundary layer under ground excitation $z_0 = 0.001 \sin(1.38 \times 2\pi t)$ m: (a) error of $z_1(t)$, (b) error of $z_2(t)$.

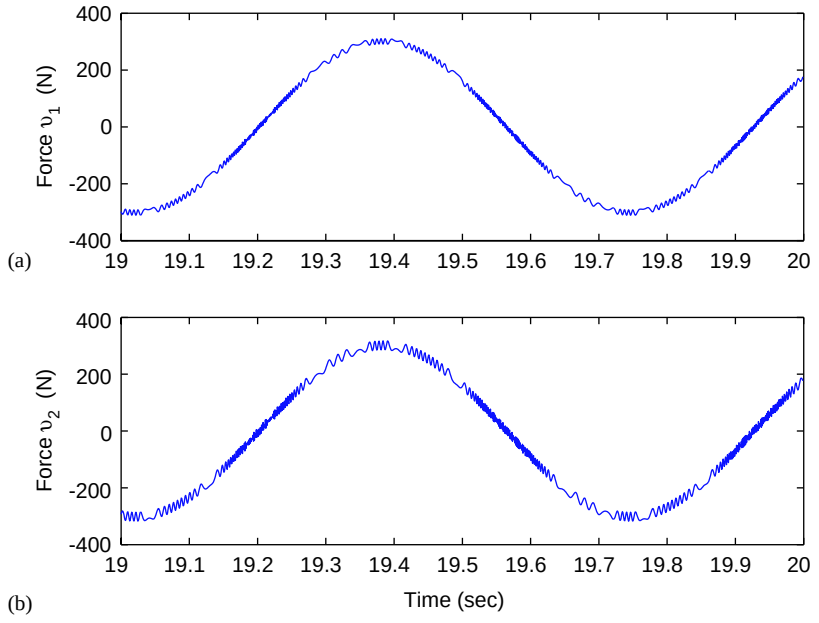

Fig. 11. Control forces with a boundary layer under ground excitation $z_0 = 0.001 \sin(1.38 \times 2\pi t)$ m: (a) force $v_1(t)$, (b) force $v_2(t)$.

The previous discussion does not include the term $\dot{x}_{i0}$ in the design of the sliding surface. If a geophone sensor is available on the ground, the frequency-shaped sliding surface (11) can be defined as

$$\sigma_i = L_i(s)(x_i - x_{i0}) + G_i(s)\dot{x}_{i0} + \dot{x}_i. \tag{33}$$

On the sliding surface, the system dynamics is (Fig. 16)

$$\frac{x_i}{x_{i0}} = \frac{L_i(s) - sG_i(s)}{s + L_i(s)}. \tag{34}$$

This system is a hybrid feedback and feedforward control. This is not surprising since the ground signals in vibration isolation are often used for feedforward. Fig. 16 suggests that we can use the extensively investigated feedback–feedforward control methods to design the frequency-shaped sliding surface. The boundary layer analysis can be carried out similarly.

5.2. Nonlinear target dynamics

We have seen that a frequency-shaped sliding surface can directly achieve target dynamics (skyhook) of the same order as the nominal plant, and we have also seen that the design of such a sliding surface turns out to be an LTI control problem of feedback or feedback–feedforward. In fact, the target dynamics can also be chosen to be nonlinear, and the sliding surface can be synthesized using contraction theory [36,37].

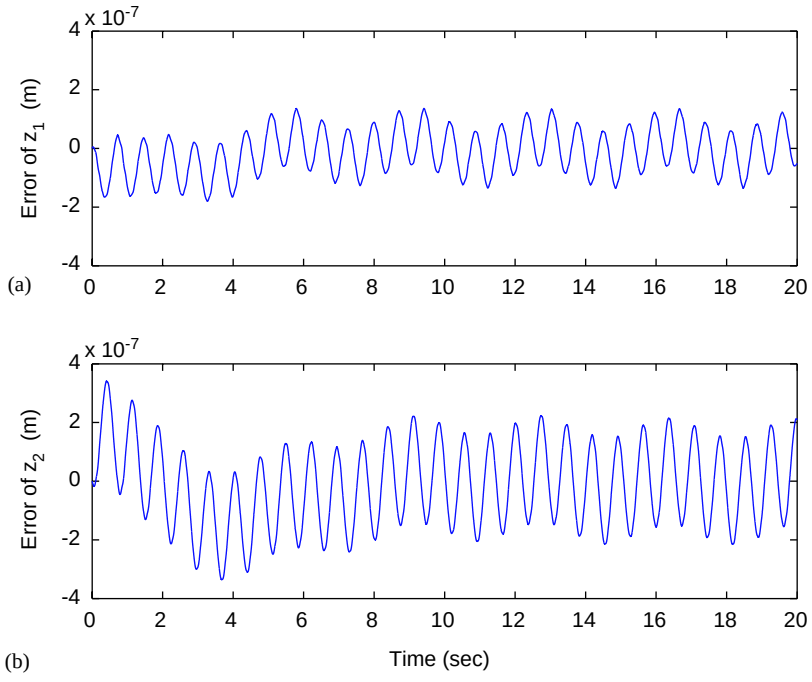

Fig. 12. Displacement errors due to a thicker boundary layer under ground excitation $z_0 = 0.001 \sin(1.38 \times 2\pi t)$ m.

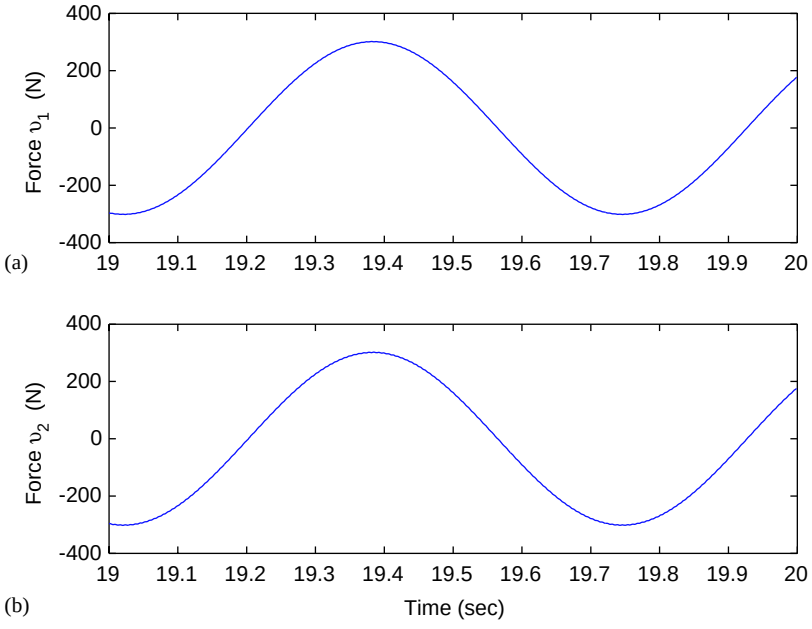

Fig. 13. Control forces with a thicker boundary layer under ground excitation $z_0 = 0.001 \sin(1.38 \times 2\pi t)$ m: (a) force $v_1(t)$, (b) force $v_2(t)$.

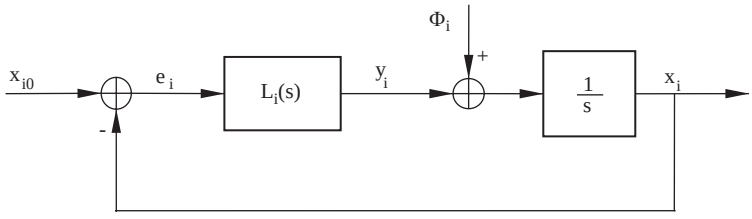

Fig. 14. Feedback system defined by sliding surface.

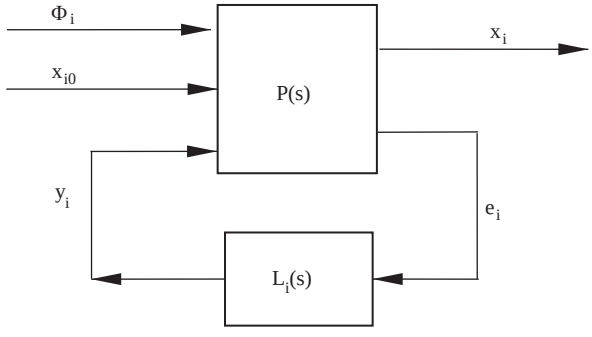

Fig. 15. Linear fraction transformation form of sliding surface.

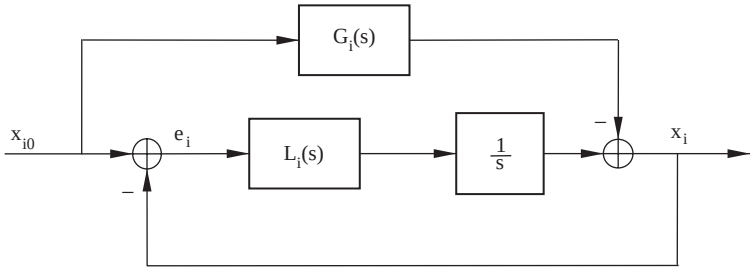

Fig. 16. Feedback–feedforward system defined by sliding surface.

Take a single-input system as example. The system to be controlled is

$$x^{(n)} = f(x, \dot{x}, \ldots, x^{(n-1)}, t) + b(x, \dot{x}, \ldots, x^{(n-1)}, t)u \tag{35}$$

and the target dynamics can be taken as any contracting system,

$$x^{(n)} = g(x, \dot{x}, \ldots, x^{(n-1)}, t). \tag{36}$$

To achieve this target, we can define the sliding surface as

$$\sigma = x^{(n-1)} + \bar{\sigma} \tag{37}$$

and

$$\dot{\bar{\sigma}} = -a(t)(\bar{\sigma} + x^{(n-1)}) - g(x, \dot{x}, \ldots, x^{(n-1)}, t), \tag{38}$$

where $a(t)$ is a time-varying or invariant gain or an operator such that $\dot{\sigma} - a(t)\sigma$ is contracting.

In this way, we construct a hierarchy of two nominally contracting systems,

$$\dot{\sigma} - a(t)\sigma = x^{(n)} - g(x, \dot{x}, \ldots, x^{(n-1)}, t), \tag{39}$$

and we can design the control u to make σ tend to zero under the plant uncertainty or disturbance.

We note that the initial condition of $\bar{\sigma}$ can be chosen as $-x^{(n-1)}$ such that σ is initially zero.

Furthermore, the target dynamics has been chosen to be of the same order as the system to be controlled. This may be natural, e.g., when the system is best controlled intermittently, or when it must follow a desired dynamic behavior rather than desired trajectory, as in some robotic locomotion applications.

5.3. Adaptive control based on frequency-shaped manifold

We also extend the frequency-shaped sliding control of vibration isolation to adaptive control [16], so that we can attain the desired multi-dof skyhook isolation without the step of identifying the modal parameters. In the following, we will summarize the adaptive control based on a frequency-shaped manifold with $f_d = 0$. For the case where f_d is not zero (but is bounded), a similar expression can be derived with some slight revision.

The matrix B in the plant dynamics (1) is determined by the geometric location of the actuators and sensors, which is relatively easy to obtain. We assume matrix B is obtained off-line, and the matrices M, C, and K are unknown. Now we would like to achieve the desired nth dof skyhook isolation in the form

$$\ddot{z} + \bar{C}\dot{z} + \bar{K}(z - z_0) = 0, \tag{40}$$

where $\bar{C}$ and $\bar{K}$ are preselected matrices to meet the requirement of frequency-domain performance.

We define a frequency-shaped manifold vector with n entries in the state space,

$$\sigma = \dot{z} + (sI + \bar{C})^{-1}\bar{K}(z - z_0). \tag{41}$$

Similar as the single mode case in Section 3, we see that the nth dof target skyhook effect (40) is achieved once the system is driven to this manifold $\sigma = 0$.

By rearranging the unknown parameters in the matrices K, C, and M into a column vector a, we write

$$K(z - z_0) + C(\dot{z} - \dot{z}_0) - M(sI + \bar{C})^{-1}\bar{K}s(z - z_0) := Ya, \tag{42}$$

where Y is a matrix with proper dimension composed of $z - z_0$, and $\dot{z} - \dot{z}_0$. Note that in Eq. (42) the unknown matrices K, C, and M show up linearly in vector a.

We choose a positive-definite Laypunov function as

$$V(\sigma, \tilde{a}) = \tfrac{1}{2}\sigma(t)^{\mathrm{T}} M\sigma(t) + \tfrac{1}{2}\tilde{a}(t)^{\mathrm{T}} P^{-1}\tilde{a}(t), \tag{43}$$

where the vector $\sigma(t)$ is defined by Eq. (41), M is the mass matrix of the system (symmetric positive definite), P is a pre-selected (constant) symmetric positive-definite matrix, and the vector of $\tilde{a}(t)$ is the error vector of on-line estimates of the parameters a, that is, $\tilde{a}(t) = \hat{a}(t) - a$.

The time derivative of $V(\sigma, \tilde{a})$ can be obtained as

$$\dot{V}(\sigma, \tilde{a}) = \sigma(t)^{\mathrm{T}}(Bu - Ya) + \dot{\tilde{a}}(t)^{\mathrm{T}} P^{-1} \tilde{a}(t). \tag{44}$$

Therefore, we obtain the control-force vector as

$$u = B^{-1}[Y\hat{a}(t) - k_d\,\sigma(t)] \tag{45}$$

and the parameter adaptation law as

$$\dot{\hat{a}}(t) = \dot{\tilde{a}} = -PY^{\mathrm{T}}\sigma(t), \tag{46}$$

such that $\dot{V}(\sigma, \tilde{a}) = -\sigma(t)^{\mathrm{T}} k_d\,\sigma(t)$ is negative semi-definite for some selected positive-definite matrix k_d of size $n \times n$, and $\ddot{V}(\sigma, \tilde{a})$ is bounded. Thus, according to the Lyapunov theorems and Barbalet's lemma [28], we conclude that $\sigma(t) \to 0$ as $t \to \infty$, and hence the target dynamics of skyhook isolation (40) is achieved.

Eqs. (45) and (46) define the adaptive control of vibration isolation based on frequency-shaped dynamic manifolds. Note that, in contrast with the well-known model reference adaptive control, the adaptive algorithm of Eqs. (45) and (46) does not use any reference model, and we eliminate the requirement of ground vibration measurement. In addition, since there are additional states in the manifold σ of Eq. (41), we can choose the initial states to improve the transient performance, $\sigma(t) \to 0$.

5.4. Experiment verifications of frequency-shaped sliding and adaptive control of isolation

The frequency-shaped sliding control and adaptive control for vibration isolation have been recently verified in Ref. [16]. The experiments are based on an sdof isolation and the setup can be found in Ref. [16]. The measurements used in control are the relative displacement and the absolute velocity of the isolated platform.

Fig. 17 shows the measured time responses using the proposed sliding control under broad-bandwidth noise excitation, where the experiment plant has a resonant frequency 12 ± 1 Hz and modal damping $18 \pm 4\%$, and the target is a skyhook isolation at 2 Hz and critical damping 0.7. From Fig. 17, we see that this controller is very effective for vibration isolation. Note that in this experiment we are unable to keep the system stable with only the linear equivalent control force (18) due the parameter uncertainties.

The frequency response controlled with the frequency-shaped sliding surface is shown in Fig. 18. This figure shows that we closely achieve the skyhook target in a large bandwidth.

In the adaptive isolation based on frequency-shaped manifold, the target is selected as a skyhook isolation at 1.2 Hz and critical damping 0.7. The time responses under a harmonic excitation are shown in Fig. 19. In this experiment the parameters of the mass, stiffness, and damping are initially taken as zero and updated according to Eq. (46). We see that the adaptive control based on a frequency-shaped manifold is very effective for vibration isolation even though

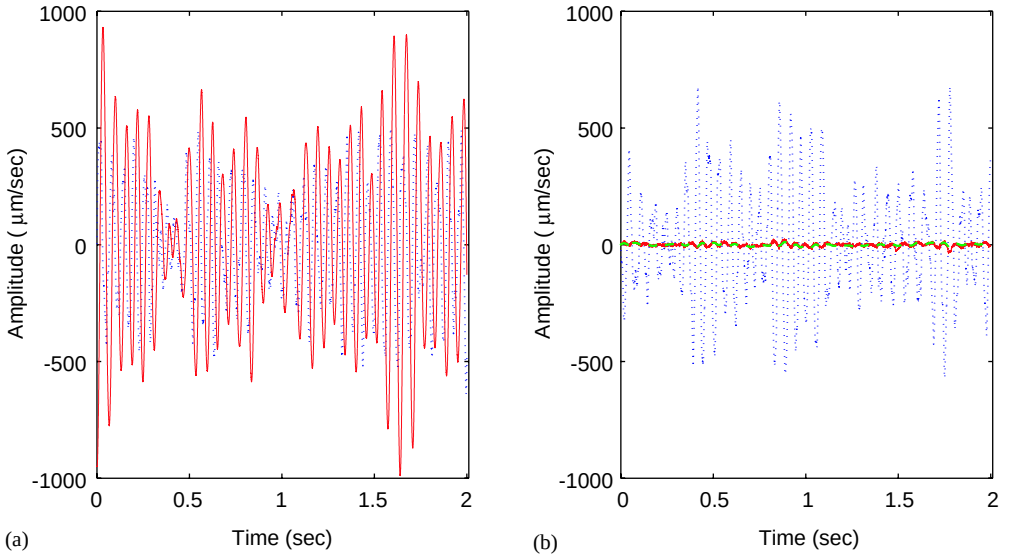

Fig. 17. Time responses of the vibration isolation system: (a) passive isolation without control, (b) active isolation with proposed sliding control. Measured base velocity (dot), measured platform velocity (solid), target skyhook velocity (dash).

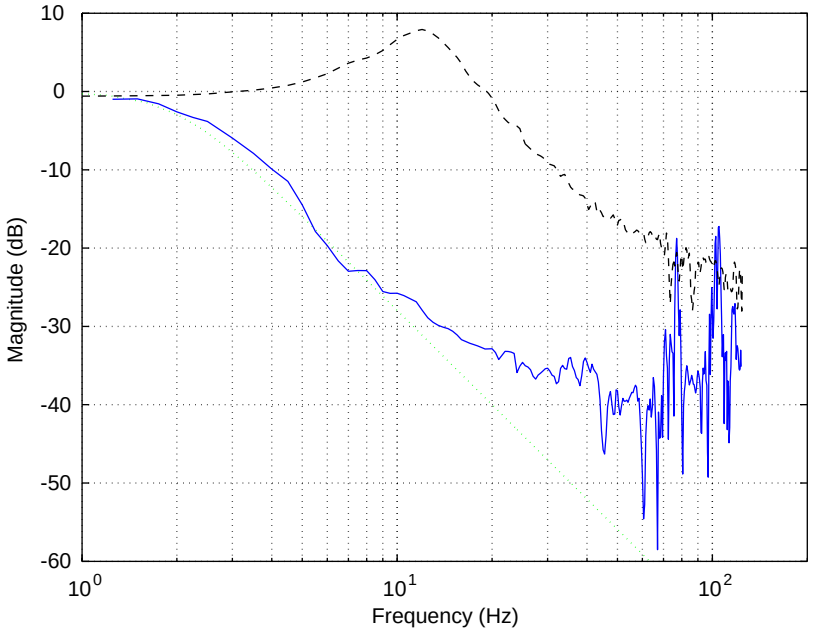

Fig. 18. Frequency responses from base velocity to platform velocity: passive isolation (dash), active isolation with the proposed sliding control (solid), skyhook target (dot).

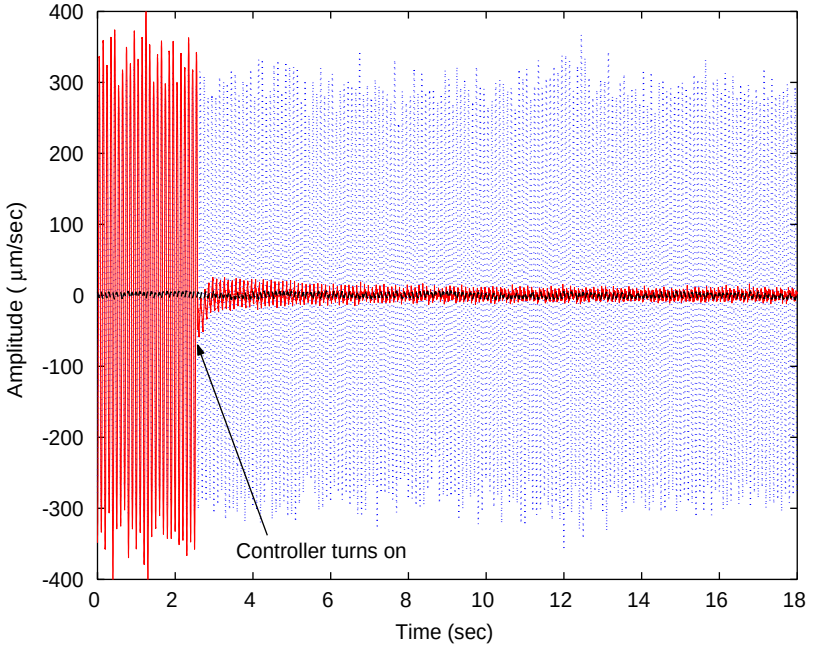

Fig. 19. Time response of single-dof isolation system (experiment) when the proposed adaptive controller turns on under 10 Hz base excitation with initial parameters set as zeros. Measured base velocity (dot), measured platform velocity (solid), target skyhook velocity (dash).

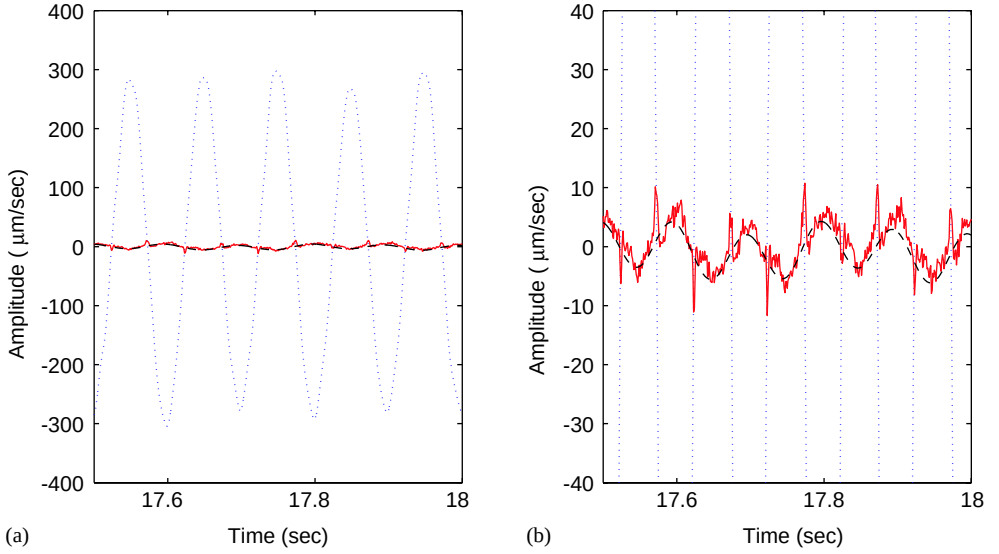

Fig. 20. Zoomed time response of isolation system with the proposed adaptive control under 10 Hz base excitation: (a) zoom in time-axis only, (b) zoom in time and amplitude axes. Measured base velocity (dot), measured platform velocity (solid), target skyhook velocity (dash).

we do not have any prior knowledge of the plant parameters. The zoomed times responses are shown in Fig. 20 in comparison with the ideal skyhook, from which we see that the skyhook target is closely approximated.

6. Concluding remarks

In this paper, we have proposed a robust control schedule for multi-dof vibration isolation. Modal decomposition is employed to handle the MIMO vibration control using the SISO control method in modal coordinate, and we can model the system from measured transfer functions via experimental modal analysis. Therefore, the proposed control schedule is applicable to controller synthesis based on measurement data or analytical modelling. Frequency-shaped sliding control, originally proposed in the literature for chattering reduction, is exploited instead to achieve performance requirements in the frequency domain under plant uncertainties and payload/upper stage disturbances. The effect of boundary layer thickness on the performance is quantified. Simulation results illustrate that we can robustly achieve the ideal skyhook effect of vibration isolation. We have also extended the frequency-shaped sliding control to a modal reaching adaptive control for vibration isolation. We further show that the design of frequency-shaped sliding surface is equivalent to a control problem of feedback or feedback–feedforward, and that linear or nonlinear target dynamics of the same order as the system to be controlled can also be attained. Recent experiments also demonstrate that the sliding and adaptive control based on a frequency-shaped sliding surface are very effective for vibration isolation.

Acknowledgements

We wish to thank Professor Samir Nayfeh of MIT for his instruction on modal testing and for his encouragement of this work. The authors also wish to thank the anonymous reviewers for their valuable comments and suggestions.

References

[1] D. Karnopp, M.J. Crosby, R.A. Harwood, Vibration control using the semi-active force generators, *ASME Journal of Engineering for Industry* 96 (1974) 619–626.

[2] D. Karnopp, Active and semi-active vibration isolation, *ASME Journal of Mechanical Design* 117 (1995) 177–185.

[3] M. Serrand, S. Elliott, Multichannel feedback control for the isolation of base-excited vibration, *Journal of Sound and Vibration* 234 (4) (2000) 681–704.

[4] A. Preumont, A. Francois, F. Bossens, A. Abu-Hanieh, Force feedback versus acceleration feedback in active vibration isolation, *Journal of Sound and Vibration* 257 (2002) 605–613.

[5] D. Hrovat, Survey of advanced suspension developments and related optimal control applications, *Automatica* 33 (10) (1997) 1781–1817.

[6] H. Yoshioka, Y. Takahashi, K. Katayama, T. Imazawa, N. Murai, An active microvibration isolation system for Hi-tech manufacturing facilities, *AMSE Journal of Vibration and Acoustics* 123 (4) (2001) 269–275.
[7] M.R. Bai, W. Liu, Control design of active vibration isolation using μ-synthesis, *Journal of Sound and Vibration* 257 (1) (2002) 157–175.
[8] B. Zhao, X. Lu, M. Wu, Z. Mei, Sliding mode control of buildings with base-isolation bybrid protective system, *Earthquake Engineering and Structural Dynamics* 29 (2000) 315–326.
[9] N. Luo, J. Rodellar, D. De la Sen, J. Vehi, Output feedback sliding mode control of base isolated structures, *Journal of the Franklin Institute* 337 (2000) 555–577.
[10] A. Alleyne, J.K. Hedrick, Nonlinear adaptive control of active suspensions, *IEEE Transactions on Control Systems Technology* 3 (1) (1995) 84–101.
[11] C. Kim, P.I. Ro, A sliding mode controller for vehicle active suspension systems with nonlinearities, *Proceedings of the Institution of Mechanical Engineers Part D, Journal of Automobile Engineering* 212 (1998) 79–92.
[12] Y.P. Wang, A. Sinha, Adaptive sliding mode control algorithm for multi-degree-of-freedom microgravity isolation system, in: *Proceedings of the IEEE International Conference on Control Applications*, 1997.
[13] K. Mizutani, Y. Fujita, H. Ohmori, Hybrid control system for microvibration isolation, in: *Proceedings of the Fourth IEEE International Workshop on Advanced Motion Control*, vol. 2, 1996, pp. 577–582.
[14] S.J. Richman, J.A. Giame, D.B. Newell, R.T. Stebbins, P.L. Bender, J.E. Faller, Multistage active vibration isolation system, *Review of Science Instruments* 69 (6) (1998) 2531–2538.
[15] K.D. Young, U. Ozguner, Frequency shaping compensator design for sliding mode, *International Journal of Control* 57 (5) (1993) 1005–1019.
[16] L. Zuo, J.J.E. Slotine, S.A. Nayfeh, Model reaching adaptive control for vibration isolation, *IEEE Transactions on Control Systems Technology* (2005) (in press).
[17] E.I. Rivin, Vibration isolation of precision equipment, *Precision Engineering* 17 (1) (1995) 41–56.
[18] Y.S. Hung, A.G.J. MacFarlane, *Multivariable Feedback: a Quasi-Classical Approach*, Springer, Berlin, 1982.
[19] L. Ljung, *System Identification: Theory for the User*, Prentice-Hall, Englewood Cliffs, NJ, 1999.
[20] J.E. Mottershead, M.I. Friswell, Model updating in structural dynamics: a survey, *Journal of Sound and Vibration* 167 (2) (1993) 347–375.
[21] D.J. Ewins, *Modal Testing: Theory*, *Practice*, *and Application*, Research Studies Press, 2000.
[22] D.J. Inman, Active modal control for smart structures, *Philosophical Transactions of the Royal Society of London Series A* 359 (2001) 205–219.
[23] M.J. Balas, Trends in large space structure control theory: fondest hopes, wildest dreams, *IEEE Transactions on Automatic Control* 27 (3) (1982) 522–535.
[24] L. Meirovitch, *Dynamics and Control of Structures*, Wiley, New York, 1990.
[25] D. Vaes, W. Souverijns, J. DeCupyper, J. Swevers, P. Sas, Optimal decoupling for improved multivariable controller design, applied on an automotive vibration test rig, in: *Proceedings of the American Control Conference*, 2003, pp. 785–790.
[26] D.H. Owens, *Multivariable and Optimal Systems*, Academic Press, New York, 1981.
[27] D.L. Trumper, T. Sato, A vibration isolation platform, *Mechantronics* 12 (2002) 281–294.
[28] J.J.E. Slotine, W. Li, *Applied Nonlinear Control*, Prentice-Hall, Englewood Cliffs, NJ, 1991.
[29] J.Y. Hung, W. Gao, J.C. Hung, Variable structure control: a survey, *IEEE Transactions on Industrial Electronics* 40 (1) (1993) 2–22.
[30] K.D. Young, V.I. Utkin, U. Ozguner, A control engineer's guide to sliding mode control, *IEEE Transactions on Control Systems Technology* 7 (3) (1999) 328–342.
[31] S.P. Chan, W. Gao, Variable structure model-reaching control strategy for robot manipulators, in: *Proceedings of the IEEE International Conference on Robotics and Automation*, 1989, pp. 1504–1508.
[32] B. Yao, M. Tomizuka, Smooth robust adaptive sliding model control of manipulators with guaranteed transient performance, *ASME Journal of Dynamic Systems, Measurement, and Control* 118 (1996) 764–775.
[33] J.J.E. Slotine, Sliding controller design for nonlinear systems, *International Journal of Control* 40 (2) (1984) 421–434.
[34] X. Chen, T. Fukuda, K.D. Young, A new nonlinear robust disturbance observer, *Systems & Control Letters* 41 (2000) 189–199.

[35] U. Stobener, L. Gaul, Active vibration control of a car body based on experimentally evaluated modal parameters, *Mechanical Systems and Signal Processing* 15 (2001) 173–188.
[36] W. Lohmiller, J.J.E. Slotine, On contraction analysis for non-linear systems, *Automatica* 34 (6) (1998) 683–696.
[37] W. Lohmiller, J.J.E. Slotine, Control system design for mechanical systems using contraction theory, *IEEE Transactions on Automatic Control* 45 (5) (2000) 984–989.